Mon. Not. R. Astron. Soc. **346,** 37–46 (2003)

The infrared–X-ray continuum correlation in active galactic nuclei

M. Contini,[1⋆] S. M. Viegas[2] and P. E. Campos[2]

[1] *School of Physics and Astronomy, Tel Aviv University, Tel Aviv 69978, Israel*
[2] *Instituto de Astronomia, Geofísica e Ciências Atmosféricas, USP, Rua do Matão 1226, 05508-900 São Paulo, Brazil*

Accepted 2003 August 1. Received 2003 July 29; in original form 2003 June 26

ABSTRACT

The correlation between the soft X-ray and near-infrared emission from active galactic nuclei (AGNs) is analysed using composite models. We find new evidence for differences in the ranges of parameters that characterize the narrow-line region (NLR) of Seyfert galaxies and low-ionization nuclear emission regions (LINERs). Soft X-rays show less variability, so they are better fitted for this kind of analysis. In our models, soft X-rays are emitted in the post-shock region of clouds with relatively high shock velocities $V_s > 250$ km s^{-1}. Consequently, dust emission peaks in the mid-infrared. On the other hand, in the photoionized zone, dust is at lower temperature and usually does not contribute to the mid-infrared emission. The results are sensible enough to allow the same modelling method to be applied to different types of AGN. We found that shock velocities are between 300 and 1000 km s^{-1}, with the NLR of low-luminosity active galactic nuclei (LLAGNs) and type 2 Seyfert galaxies (Sy2s) showing lower velocities than type 1 Seyfert galaxies (Sy1s). The intensity of the ionizing radiation flux at the Lyman limit from the central source is low for LINERs and low-luminosity AGNs ($\log F_h = 9$ to 10), increasing towards Sy2s ($\log F_h \sim 11$) and Sy1s ($11 \leqslant F_h \leqslant 12$). Results obtained by modelling the *Einstein* and the *ROSAT* samples of galaxies are in full agreement. Dust-to-gas ratios by number are $\geqslant 10^{-14}$ in LINERs and LLAGNs, between 10^{-15} and 3×10^{-13} in Sy1s and up to 5×10^{-13} in Sy2s. In order to fit the infrared and X-ray continua, an η factor is defined, which accounts for the emitting area of the cloud. If the infrared emission is due to bremsstrahlung and comes from the same cloud that produces the soft X-rays, the η values obtained from both emissions must be the same. Therefore, if $(\eta)_{IR} < (\eta)_{soft\,X}$, there must be a strong contribution of soft X-rays from the active centre. From the η values, we expect to identify the objects that could present strong variability.

Key words: radiation mechanisms: non-thermal – shock waves – galaxies: Seyfert – infrared: galaxies – X-rays: galaxies.

1 INTRODUCTION

The main source of ionization and heating of the emission-line region in active galactic nuclei (AGNs) is photoionization by radiation from the active centre (AC). Nevertheless, the contribution of shock waves, generated by the radial motion of the clouds or associated with jets, to the emission originating in the narrow-line region (NLR) of type 1 Seyfert galaxies (Sy1s), type 2 Seyfert galaxies (Sy2s) and low-ionization nuclear emission regions (LINERs) has been pointed out, for example, by Viegas & de Gouveia dal Pino (1992), Contini (1997) and Contini & Viegas (2001), and more recently by authors analysing the soft X-ray spectrum of AGN (e.g. Iwasawa et al. 2003). The relative importance of shocks and radiation can be roughly evaluated in the different objects, because these processes act in different domains. In fact, shocks heat the gas within the clouds to high temperatures in the downstream region, so they can easily explain the observed high ionization lines (Rodriguez-Ardila et al. 2002) and soft X-ray emission (Contini, Viegas & Prieto 2002, and references therein).

Indeed, if soft X-rays are emitted by bremsstrahlung from the NLR clouds, the gas temperature must be at least of the order 10^6 K. Such temperatures are obtained in the post-shock region if the shock velocity is higher than 250 km s^{-1}. The full width at half-maximum (FWHM) of the line profiles in the NLR of Sy2s and Sy1s indicate that the cloud velocities can well be beyond this range. Modelling the emission-line and continuum spectra of some Sy2s (e.g. NGC 5252, Circinus, NGC 4151) indicates the presence of very high shock velocities, which can provide a thermal origin for the observed soft X-rays.

Based on early observations of different galaxies by *EXOSAT*, the nature and variability of soft X-rays was investigated, revealing a

⋆E-mail: contini@ccsg.tau.ac.il

low and long-term variability compatible with bremsstrahlung emission from a hot gas. For instance, Pounds et al. (1986) showed the existence of a soft X-ray spectral component, distinguished from the main (nuclear) X-ray emission of NGC 4151 by a lack of variability. This component is shown to be consistent with thermal emission from a hot, confining medium in the region of the narrow emission-line clouds. Perhaps NGC 4151 is an exception to the general rule that soft X-ray emission from AGNs is variable, because most of its soft X-ray flux is absorbed by a high intrinsic column density, so that its faint, diffuse X-ray flux can be detected. This effect should not appear in most objects.

The correlation between the soft X-ray and infrared (IR) luminosities in AGN has been studied by several authors and is controversial. One important issue is the source of variability in the various frequency ranges. In particular, the correlations of $L_{\rm X}$ (0.5–4.5 keV) versus $L_{\rm IR}$ for the IRAS 12, 25, 60 and 100 μm bands have been examined by Green, Anderson & Ward (1992). They claim that $L_{\rm X}$ versus $L_{25\,\mu{\rm m}}$ and $L_{\rm X}$ versus $L_{100\,\mu{\rm m}}$ resemble very closely the $L_{\rm X}$ versus $L_{60\,\mu{\rm m}}$ correlation and that the plot of $L_{\rm X}$ versus $L_{12\,\mu{\rm m}}$ is considerably better defined, yet, just as in the $L_{60\,\mu{\rm m}}$ plot, 'Seyfert galaxies still show no significant correlation' (Green et al. 1992, fig. 3).

On the other hand, the correlation between the 10 μm and the hard X-ray emission showed opposite results (Carleton et al. 1987; Giuricin et al. 1994) and was reanalysed by Giuricin, Mardirossian & Mezzetti (1995). They obtained a weak correlation with a harder (2–10 keV) X-ray emission, mainly induced by Sy2 data. They also found that the 10 μm emission correlates well with the 12 and 25 μm, and less well with the far-infrared emission at 60 and 100 μm. These authors favour thermal emission as the origin of the mid-infrared emission of Seyfert galaxies.

Dust is present in the NLR clouds and re-emission by grains may dominate the IR domain. If the intense ultraviolet–optical central radiation heating the nuclear dust has an X-ray counterpart, a correlation between the infrared and X-ray emission should be expected (Barvainis 1990). Because in shocked zones the dust grains are usually heated to higher temperatures than in photoionized regions, the contribution from the shocked NLR clouds probably dominates the near-infrared emission. A contribution to the IR from bremsstrahlung emission from a cooler gas is not excluded and would result in a correlation between the soft X-ray and the near-IR continua. Nevertheless, in the former case the mutual heating of dust and gas (Viegas & Contini 1994) can also lead to a correlation between those two continua. Therefore, in both cases a correlation is expected. Notice that the contribution of a dusty torus to the IR emission suggested by the AGN unified model (Antonucci & Miller 1985) will give poor or no correlation with the soft X-ray emission as pointed out by Green et al. (1992) (see also Contini, Viegas & Prieto, in preparation, and references therein).

A major problem concerning correlations between X-ray and IR emission is X-ray variability. It is well established that soft X-rays from low-luminosity active galactic nuclei (LLAGNs) and LINERs show less and/or longer variability than the hard X-rays (Halderson et al. 2001; Terashima, Ho & Ptak 2000). Following Green et al. (1992), we will therefore analyse the possible correlation between mid-IR ($L_{12\,\mu{\rm m}}$) and X-rays for these galaxies, which present a bolometric luminosity that can be several orders of magnitude lower than the brightest AGN.

Notice that 10 μm falls in the absorption trough of the spectral energy distribution due to silicate grains. On the other hand, polycyclic aromatic hydrocarbon (PAH) emission bands dominate the infrared spectral energy distribution (SED) of galaxies at 6.2, 7.7, 8.6, 11.3 and 12.7 μm (Spoon et al. 2002). However, PAH grains are small compared with silicate grains and easily sputtered in AGN, where shock velocities are high enough ($\geqslant$300 km s^{-1}). Therefore, we refer in this paper to the 12 μm emission in the mid-IR.

It was found in previous investigations on the Seyfert galaxies, NGC 5252 (Contini, Prieto & Viegas 1998a), Circinus (Contini, Prieto & Viegas 1998b) and NGC 4151 (Contini et al. 2002), that the critical shock velocity ($V_{\rm s}$) to produce dust emission in the mid-IR is of the order of 500 km s^{-1} (Viegas & Contini 1994), and that the critical $V_{\rm s}$ for soft X-ray emission, fitting most of our sample for type 2 Seyfert galaxies, is about 1000 km s^{-1} (Contini & Viegas 2000). However, the dust-to-gas ratio, d/g, may change from galaxy to galaxy, as well as in the different regions of a single galaxy. Therefore a scattering of the infrared data for a sample of galaxies is expected.

The FWHM of the line profiles is lower in LINERs ($<$300 km s^{-1}) than in Seyfert galaxies (300 to 500 km s^{-1}). Notice, however, that broad Hα lines have been observed from LINERs (Ho, Filippenko & Sargent 1997), indicating that clouds with higher velocities may also contribute to the spectra. Therefore, in these objects, characterized by a low ionizing flux from the AC, shocks are relatively important and may contribute to both the near-IR and soft X-ray emission. The observed data will be confronted to model results obtained by numerical simulations with the SUMA code (Viegas & Contini 1994; Contini & Viegas 2001), which accounts for both the shock and photoionization effects in the NLR clouds.

Once tested for the low-luminosity objects, in the second part of this paper we will apply the same kind of analysis to Seyfert galaxies. We will restrict the data to the soft X-ray part of the spectrum, where the variability is not as strong as in the hard X-rays. From the comparison with model results, we expect to select those galaxies where the contribution to soft X-rays from the AC prevails, indicating in this way the objects of the sample which should show a higher degree of variability.

The SED of dust and gas emissions obtained from the models, as well as the corresponding temperatures of the dust grains, are discussed in Section 2. The $L_{\rm X}$–$L_{12\,\mu{\rm m}}$ correlation for LLAGNs and LINERs is investigated in Section 3, while that for Seyfert galaxies is discussed in Section 4. Concluding remarks appear in Section 5.

2 GAS AND DUST EMISSIONS

2.1 The model

In our model the nuclear clouds are moving outward from the AC. A shock front appears at the cloud outer edge, while radiation from the AC reaches the inner edge. The physical conditions of an emitting cloud due to the coupled effect of shock and photoionization by a radiation source are obtained with the SUMA code assuming a plane-parallel symmetry. The calculations start at the shocked edge. In the first run, only the shock effect is accounted for, and the physical conditions are obtained for several ($\leqslant$300) slabs before reaching the opposite edge. In this first run the results correspond to a shock-dominated model. Iterative runs start alternately at the photoionized and shocked edges, accounting for both effects, until convergence of the physical conditions in the cloud is achieved.

The input parameters for a single-cloud model are the shock velocity, $V_{\rm s}$, the pre-shock density, n_0, the pre-shock magnetic field, B_0, the ionizing radiation spectrum, the chemical abundances, the dust-to-gas ratio by number, d/g, and the geometric thickness of the clouds, D. A power law is adopted for the central ionizing radiation spectrum reaching the cloud, characterized by the flux $F_{\rm h}$,

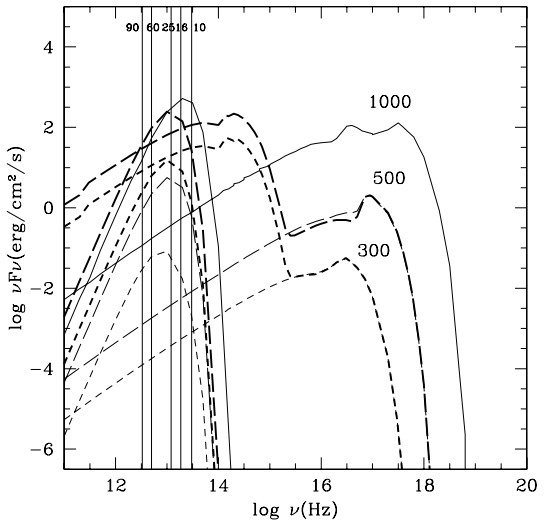

Figure 1. The SED of the continua emitted by bremsstrahlung and by dust from the clouds. Long-dashed lines refer to $V_s = 500$ km s^{-1}, log $F_h = 12$; short-dashed lines to $V_s = 300$ km s^{-1}, log $F_h = 11$; solid lines to $V_s = 1000$ km s^{-1}. Thick lines represent RD models, thin lines are SD models. The vertical lines correspond to the main IR observed wavelengths.

at the Lyman limit (in units of cm^{-2} s^{-1} eV^{-1}) and the power-law index α ($F_h \propto \nu^{-\alpha}$). For all the models, $B_0 = 10^{-4}$ G, $\alpha_{UV} = 1.5$ and $\alpha_X = 0.4$, and cosmic abundances (Allen 1973) are adopted. The model is either radiation-dominated (RD) or shock-dominated (SD) depending on the intensity of the ionizing flux and on the shock velocity (Viegas-Aldrovandi & Contini 1989). For SD models $F_h = 0$.

The gas entering the shock front is thermalized and heated. Depending on the shock velocity, a high-temperature zone can be produced where soft X-rays are generated by bremsstrahlung. A lower-temperature zone may produce near infrared emission by the same mechanism. The temperature of the photoionized zone is never too high ($<4 \times 10^4$ K), thus its bremsstrahlung emission is mainly in the IR–optical range, depending on the intensity of the ionizing radiation. Thermal emission from dust grains could also produce near-IR emission, as long as the dust temperature is high enough as discussed below.

Before discussing the temperature of the grains, let us illustrate the SED of the continuum, accounting for both gas bremsstrahlung and dust re-emission calculated by a composite model (Contini & Viegas 2000). The SEDs shown in Fig. 1 correspond to single-cloud models with various cloud velocities and ionizing radiation intensities, assuming a geometric thickness of the cloud $D = 10^{19}$ cm and dust-to-gas ratio $d/g = 10^{-14}$ by number (or 4×10^{-4} by mass, adopting silicate grains). Following the results obtained in our previous papers, models with high velocities (1000 km s^{-1}) are SD, because the effect of the shock prevails on photoionization from the AC. The results shown in Fig. 1 will help to understand the soft X-ray emission radiation from clouds in the physical conditions suitable to those in the NLR of AGNs and in LINERs.

2.2 The temperature of the dust grains

The dust temperatures calculated by models with $V_s = 300$ and 1000 km s^{-1} are presented in Table 1, for both the SD side and the RD side of the single clouds. We assume that grains are present inside the whole cloud before entering the shock front and all the dust grains have initially the same size a_{gr}. The grain radius may change due to sputtering. A dust-to-gas ratio $d/g = 10^{-14}$ by number is adopted.

Table 1. Model results: the temperature of grains.

log F_h	V_s (km s^{-1})	n_0 (cm^{-3})	a_{gr} (μm)	T_{gr}(SD) (K)	T_{gr}(RD) (K)
–	1000	1000	0.5	318	–
11	300	300	0.5	154	55.2
–	1000	1000	0.2	147	–
11	300	300	0.2	165	55.8
–	1000	1000	0.01	–	–
11	300	300	0.01	168	69.7
12.7	300	300	0.01	168	112

In the photoionized zone, sputtering is not important and the grain temperature increases with decreasing grain radius and increasing F_h. The behaviour is rather different in the shocked zone because of sputtering throughout the shock front. The higher V_s, the stronger the sputtering and the higher the grain temperature, as long as the grains survive sputtering. So, larger grains, which survive sputtering through high-velocity shock fronts, show a distribution of different radius throughout the cloud. They reach higher temperatures and the peak of dust thermal emission shifts towards higher frequencies. This peak can be high depending on the volume of the dusty region. When the grain initial radius is small and the shock velocity high, the dust grains are destroyed by sputtering, so dust cannot survive in the SD side of the cloud (see Contini et al., in preparation). Moreover, there is a mutual heating between gas and dust (see Viegas & Contini 1994).

It can be seen that T_{gr} in the RD zone is always lower than in the SD zone, even for small grains ($a_{gr} = 0.01\,\mu$m) and high F_h (5×10^{12} cm^{-2} s^{-1} eV^{-1}). On the other hand, dust is destroyed by sputtering if the initial grain radius is low and V_s is high, as exemplified by the model with $a_{gr} = 0.01$ μm and $V_s = 1000$ km s^{-1}.

In brief, if the mid-infrared emission of AGN, particularly the 12-μm emission, is thermal emission due to grains, the grains must be heated in a shocked zone.

3 LOW-LUMINOSITY AGNs

The correlation between the near-IR and the soft X-rays for LLAGNs is analysed using 36 nearby objects from the Halderson et al. (2001) sample. Most of the X-ray data come from observations with *ROSAT*, while the infrared data are from *IRAS*. Some of the objects are also included in the Terashima et al. (2002) sample of LLAGNs observed with *ASCA*. Short-term variability ($\leqslant$1 d) was found in NGC 3031, 4258 and 5033. Long-term variability is observed in NGC 3031, 4258 and 4579, while no significant variability was found in NGC 404, 4111, 4438, 4579 and 4639.

The correlation between the 12 μm and soft X-rays for LLAGNs is shown in Fig. 2, where we plot the ratio of the IR and X-ray observed fluxes versus the X-ray luminosity. The choice of the vertical axis is explained below, where we compare the observational data with the results of numerical simulations.

3.1 Modelling the sample

The single-cloud model provides the continuum and emission-line fluxes calculated at the cloud. Thus, in order to obtain the luminosities, the model results must be multiplied by a factor η accounting for the emitting area. Assuming that the single-cloud conditions correspond to the gas around the central source, the emitting area can be related to the distance of the cloud to the central source and to the

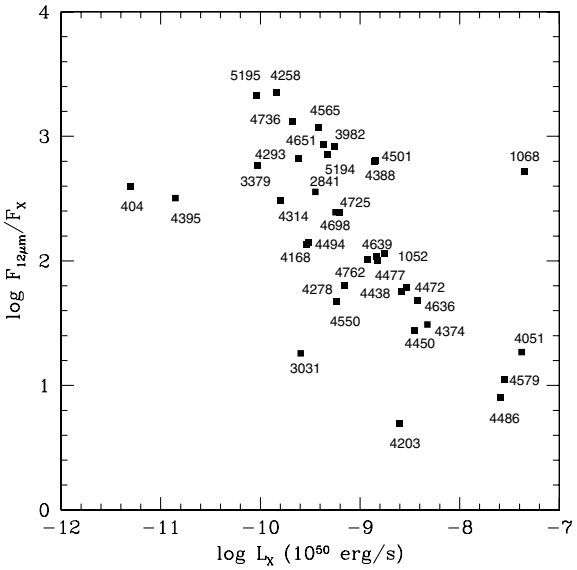

Figure 2. The ratio of the 12 μ luminosity to the soft X-ray luminosity versus the soft X-ray luminosity for the low-luminosity active galaxies of the Halderson et al. (2001) sample.

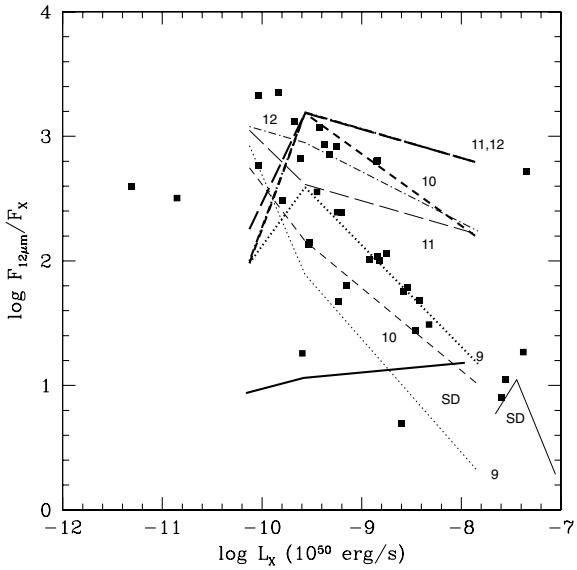

Figure 3. The comparison of model calculations with the observational data. The results of the models with different values of V_s and the same log F_h are joined by dotted (log $F_h = 9$), short-dashed log $F_h = 10$), long-dashed (log $F_h = 11$) and dash-dotted (log $F_h = 12$) lines. Solid lines correspond to shock-dominated (SD) models calculated with $F_h = 0$. Thin lines refer to bremsstrahlung emission at 12 μm, while thick lines refer to dust emission at 12 μm. The value of V_s increases from left to right.

covering factor (see, for instance, Contini & Viegas 2000). Plotting a flux ratio versus a luminosity, as in Fig. 2, this factor will affect only the horizontal axis, and the match of the models to the data would be easier, if IR and X-ray emission come from the same cloud and there is a negligible contribution of X-rays from the central source.

Since we assume that the soft X-rays come from the shocked edge of the NLR clouds, the post-shocked zone must reach temperatures higher than 10^5 K and a minimum shock velocity of 300 km s^{-1} is required. Based on previous work, a grid of models with $V_s = 300$ km s^{-1}, $n_0 = 300$ cm^{-3}, or $V_s = 500$ km s^{-1}, $n_0 = 300$ cm^{-3}, or $V_s = 700$ km s^{-1}, $n_0 = 500$cm^{-3}, and log $F_h = 9$, 10, 11, 12 was obtained for clouds with a dust-to-gas ratio of 10^{-14}, a geometrical width of $D = 10^{19}$ cm, a pre-shock magnetic field of $B_0 = 10^{-4}$ G and initial grain radius of 0.2 μm. Notice that log $F_h = 12$ is an upper limit since a low radiation flux from the AC is characteristic of LLAGNs.

Model results and observational data are compared in Fig. 3. The lines join results of models with different values of V_s but the same F_h.

The observations of the galaxies NGC 4486, 4579 and 4051 are better explained by SD models (thin solid line joining the results for $V_s = 900$, 1000 and 1100 km s^{-1} and $d/g = 10^{-13}$). Only the bremsstrahlung is shown in this case, because at these high velocities the grains are mostly destroyed by sputtering. The $F_{12\mu m}/F_X$ ratios for SD models calculated with $V_s = 300$, 500 and 700 km s^{-1} and $d/g = 10^{-14}$ are too low. Higher values (thick solid line) are obtained assuming $d/g = 2 \times 10^{-13}$.

The observed correlation is reproduced by models calculated with log $F_h = 9$ and 10. However, it is difficult to distinguish between bremsstrahlung and thermal emission by dust.

Assuming all clouds are at the same distance (r) from the centre with covering factor equal to unity, the best general fit to the observations, which reproduces the slope of the correlation, is obtained with clouds at $r = 15.45$ pc.

3.2 Results for individual galaxies

Single-cloud models for the galaxies in the sample of Halderson et al. (2001) are chosen based on two data: infrared luminosity at 12 μm, and that in soft X-rays (0.5–2.4 keV). In recent years point-to-point observations of single objects have permitted information to be obtained about the distribution of velocities, densities, intensity of the radiation from the AC, and dust-to-gas ratios throughout the galaxy. By modelling the soft X-ray continuum, however, we select clouds with shock velocities high enough to heat the gas in the post-shock region to high temperatures. The modelling of these clouds permits one to evaluate roughly their distances from the AC. In Table 2, for each galaxy of the sample the average characteristics of the emitting clouds reproducing the observed correlation are listed.

The galaxies of the Halderson et al. sample are separated into LINERs (empty squares) and LLAGNs (full squares) in Fig. 4. Some of the curves representing the results from models shown in Fig. 3 appear horizontally shifted in Fig. 4 in order to reach most of the objects. This shift corresponds to an η factor different from that used in Fig. 3. As seen in Fig. 4 most of the LINERs are fitted by low F_h (log $F_h = 9$–10), confirming that low F_h are characteristic of these objects (Contini 1997). The clouds in NGC 404 and 4395 that are closer to the AC are reached by a rather high flux (log $F_h = 11$). Our results suggest that NGC 4168 should be classified as a LINER. NGC 3031 has shock-dominated clouds close to the nucleus ($r =$ 2.4 pc) heated by a high-velocity shock ($V_s = 700$ km s^{-1}). NGC 1068, on the other hand, shows IR emission by dust from clouds with $d/g = 10^{-14}$ and $V_s = 700$ km s^{-1}, located at 23.6 pc from the centre. Clouds in NGC 4486 and 4579 have the highest shock velocities ($V_s \sim 1000$ km s^{-1}) and are located in the nuclear region ($r = 8.9$ pc). Notice that NGC 1068, which has an Hα luminosity greater than the limit for LLAGNs (10^{40} erg s^{-1}), does not follow the general trend (see Fig. 2), since high-velocity clouds at large distance from the centre are required to account for the observed L_X (Table 2). NGC 4051 is a warm absorber and soft X-ray emission has been explained by a more complete model (Contini & Viegas 1999).

Table 2. The characteristics of LLAGNs.

NGC	Class	V_s (km s^{-1})	n_0 (cm^{-3})	log F_h	d/g (10^{-14})	r (pc)
404	L2	500	300	11	1	1.5
1052	L1.9	500–700	300–500	10	1	15.5
1068	S1.9	700	500	11	1	23.6
2841	L2	500	300	9	1	15.5
3031	S1.5	700	500	SD	20	2.4
3379	L2	300	300	9	br	15.5
3982	S1.9	500–700	300–500	10–12	1–br	15.5
4051	S1.2	1000	500	SD	br	15.5
4168	S1.9	500	300	10	br	15.5
4203	L1.9	500–700	300–500	9	br	>15.5
4258	S1.9	500	300	12	1	8.9
4278	L1.9	500–700	300–500	10	br	15.5
4293	L2	300–500	300	10	1	15.5
4314	L2	300–500	300	10	br	15.5
4374	L2	500–700	300–500	9	1	15.5
4388	S1.9	500–700	300–500	10	1	15.5
4395	S1.8	500–700	300–500	11	1	1.55
4438	L1.9	500–700	300–500	9	1	15.5
4450	L1.9	500–700	300–500	10	br	15.5
4472	S2	500–700	300–500	9	1	15.5
4477	S2	500–700	300–500	9	1	15.5
4486	L2	900	500	SD	br	8.9
4494	L2	500	300	10	br	15.5
4501	S2	500–700	300–500	10	1	15.5
4550	L2	>500	>300	9	br	15.5
4565	S1.9	>500	>300	10–12	1	15.5–8.9
4579	S1.9	1000	500	SD	br	8.9
4636	L1.9	<700	<500	9	1	15.5
4639	S1.0	500–700	300–500	9	1	15.5
4651	L2	500	300	12	br	15.5
4698	S2	>500	>300	9	1	15.5
4725	S2	>500	>300	9	1	15.5
4736	L2	>500	>300	12	1	8.9
4762	L2	500–700	300–500	9	1	15.5
5194	S2	>500	>300	12	br	15.5
5195	L2	500	300	12	1	8.9

3.3 Composite radio emission

Before concluding the analysis of the LLAGN, we would like to strengthen the fact that shocks and the ionizing radiation from the AC act together in heating and ionizing the gas also in low-luminosity objects as illustrated by the radio continuum. In fact, the trend of the SED in the radio domain is obtained by summing up the contribution from the synchrotron radiation created by the Fermi mechanism at the shock front and the bremsstrahlung from the cooler cloud zones.

A few examples appear in Fig. 5, showing model results and observational data for the galaxies NGC 4258 (top panel), NGC 4278 (middle panel) and NGC 4374 (bottom panel). The model input parameters are listed in Table 2. The observational data were found in the NASA Extragalactic Database (NED) and come from Heeschen & Wade (1964), Gower, Scott & Wills (1967), Ekers (1969), Kellermann, Pauliny-Toth & Williams (1969), Dressel & Condon (1978), Laing & Peacock (1980), Kuhr et al. (1981), Large et al. (1981), Condon et al. (1983), Ficarra, Grueff & Tomasetti (1985), Israel & Mahoney (1990), Wright & Otrupcek (1990), Becker, White & Edwards (1991), Gregory & Condon (1991), White & Becker (1992), Becker, White & Helfand (1995), Douglas et al. (1996) and Waldram et al. (1996).

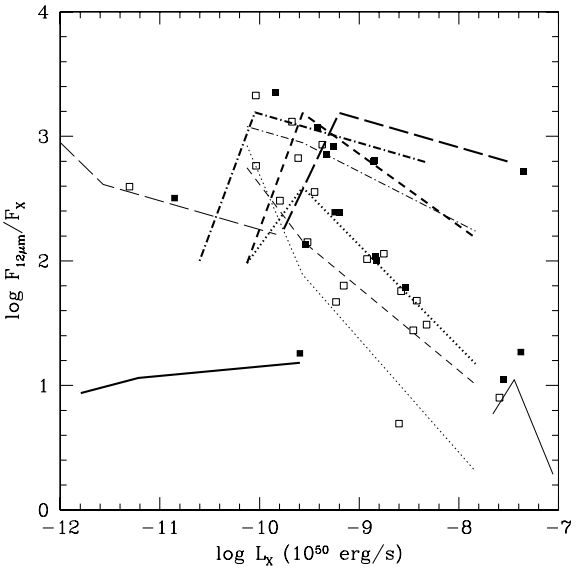

Figure 4. The best fit of the data by model results (see text).

4 THE L_X–L_{12} μm CORRELATION FOR SEYFERT GALAXIES

In this section the correlation between the soft X-ray luminosity (L_X) and the 12 μm luminosity ($L_{12\mu m}$) is investigated for a relatively large sample of Seyfert galaxies, which includes objects with higher luminosities relative to those of LINERs and LLAGNs studied in the previous sections.

We have collected a sample of 31 Sy1s and 19 Sy2s observed with the *Einstein* (0.5–4 keV band) and *IRAS* satellites. Another sample includes 26 Sy1s, 8 Sy1.5s and 10 Sy2s observed with *ROSAT* (0.5–2.4 keV). The *Einstein* data come from Green et al. (1992), the *ROSAT* data were taken from Moran, Halpern & Helfand (1996), and the *IRAS* data come from NED. The luminosities are calculated assuming a Hubble constant equal to 50 km s^{-1} Mpc^{-1}.

The correlations between $L_{12\mu m}/L_X$ and L_X for Sy1s and Sy2s are shown in Fig. 6 using *Einstein* (top panel) and *ROSAT* data (bottom panel), respectively. For comparison, the LLAGN data (Halderson et al. 2001) are also plotted. As expected the LLAGN are fainter in X-rays than the Seyfert galaxies. As expected, NGC 1068, included in the Halderson et al. sample, is located in the Seyfert galaxy zone.

The separation between the two classes of objects is more clearly marked for *ROSAT* data. The $L_{12\mu m}/L_X$ ratios are roughly of the same order. These ratios depend mainly on the dust-to-gas ratio and on the physical conditions in the NLR, indicating that the conditions are similar in the two classes of galaxies.

The same series of models (same notations) applied to the LLAGN in Fig. 3 are used to roughly model the Seyfert galaxies. In order to fit the data for the *Einstein* sample, we adopted an η corresponding to an average distance of the clouds from the AC of ∼460 pc for Sy1s and ∼90 pc for Sy2s. This corresponds to shifting the model ensemble to the right-hand side in the diagram. However, to find the best fit for Sy2s, we had to shift the models upwards by a factor of 30. The vertical axis corresponds to the $L_{12\mu m}/L_X$ ratio, where $L_{12\mu m}$ represents dust emission. Therefore, the best fit corresponds to dust-to-gas ratios higher by a factor of 30 ($d/g = 3 \times 10^{-13}$) and already suggests that the NLR of Sy2s is dustier than that of Sy1s. The same parameters used for the *Einstein* sample are adopted to fit the *ROSAT* sample (Fig. 6, bottom). Notice that Mrk

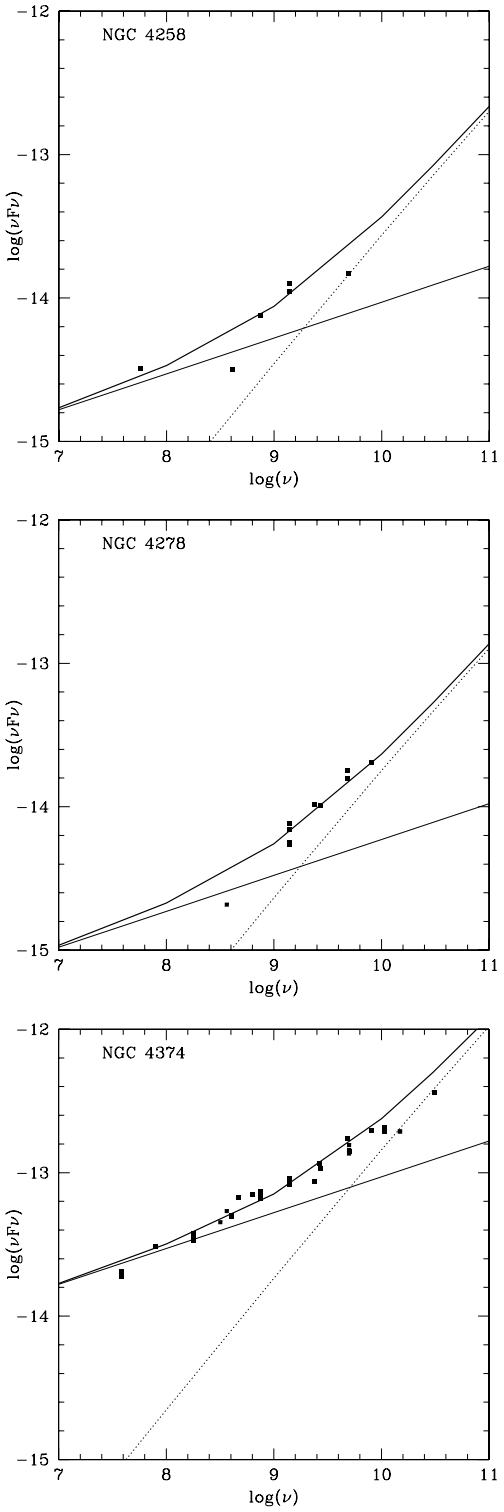

Figure 5. The calculated radio continuum for NGC 4258, 4278 and 4374. Two components are shown: the power law due to the Fermi mechanism (thin solid line) and the bremsstrahlung from a cool gas (dotted line). The thick solid line corresponds to the sum of the two components.

335, NGC 1365 and NGC 1566 from the *Einstein* sample, showing low L_X, should be classified as Sy2s rather than Sy1s.

The fit shown in Fig. 6 is reasonable, although more refined modelling is necessary. This will be done in the next section, where the

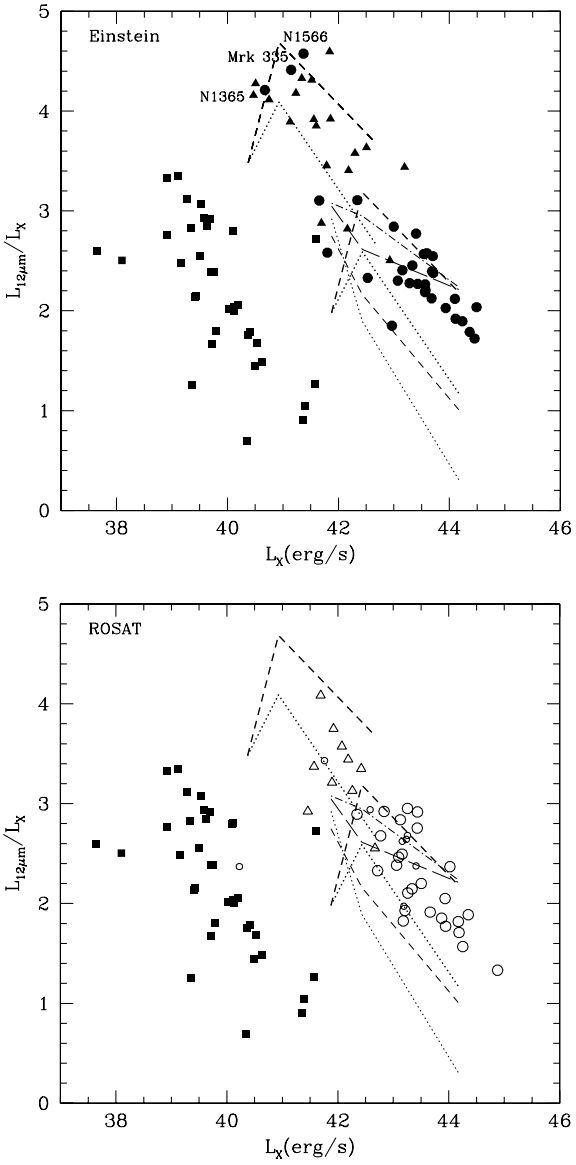

Figure 6. Top panel: $L_{12\,\mu m}/L_X$ versus L_X for Sy1s (filled circles) and Sy2s (filled triangles) using *Einstein* data. Bottom panel: $L_{12\,\mu m}/L_X$ versus L_X for Sy1s (open circles) and Sy2s (open triangles) using *ROSAT* data. In both panels, filled squares represent the LLAGNs and the lines correspond to model results with the same notation used in Fig. 3.

NLR physical conditions, as well as the evaluation of the distances of the Sy1 and Sy2 emitting clouds to the centre, are discussed. For this, the $L_{12\,\mu m}$ versus L_X correlation is used for both Sy1 and Sy2 galaxies (Figs 7 and 8, respectively, corresponding to the *Einstein* and *ROSAT* data).

4.1 Modelling the correlation

Single-cloud models that better reproduce the L_{IR}–L_X correlation shown in Figs 7 and 8 are chosen from a grid of models. All models are calculated with $d/g = 10^{-15}$ by number, $B_0 = 10^{-4}$ G and $n_0 =$ 300, 500 and 1000 cm^{-3} for models with $V_s = 300$, 500 and 1000 km s^{-1}, respectively (cf. Fig. 1). Usually in the NLR the decreasing radiation flux with the distance to the AC is followed by a decreasing velocity field. Moreover, we adopted a low dust-to-gas ratio as a

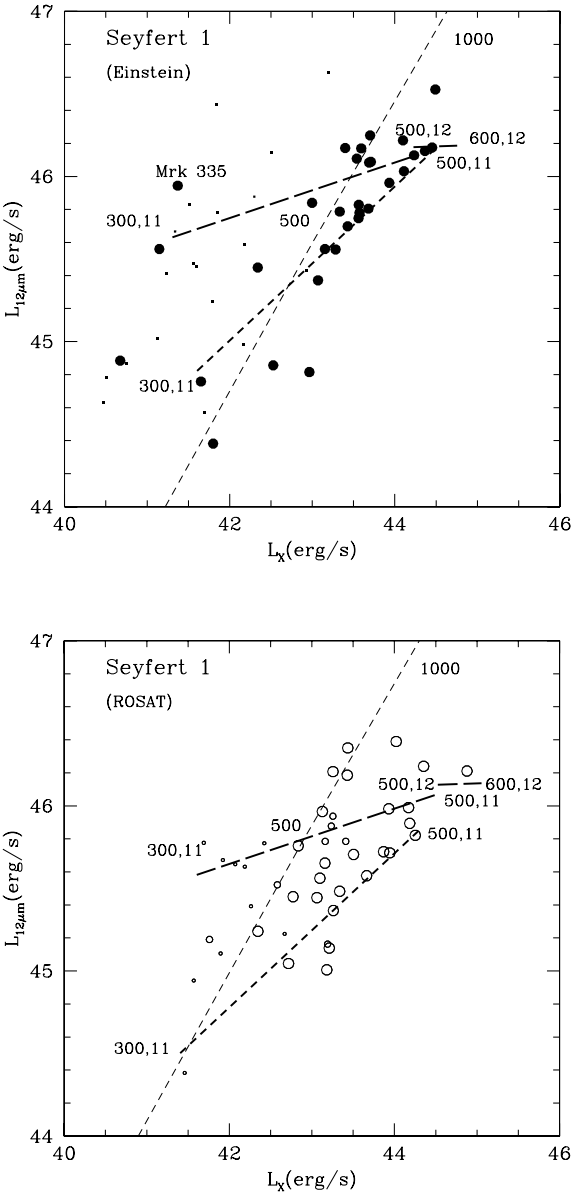

Figure 7. $L_{12\,\mu m}$ versus L_X for Sy1 galaxies (larger symbols). The top panel refers to the *Einstein* sample, while the bottom panel to *ROSAT* sample. The curves are labelled by V_s and log F_h values for RD models and by V_s for SD models. The line types are given in Tables 3 and 4 (last column). The notation for the data is as follows: *Einstein* – filled circles represent Sy1s; *ROSAT* – open circles represent Sy1s, and small open circles represent Sy1.5s; in both panels, tiny symbols correspond to Sy2 data.

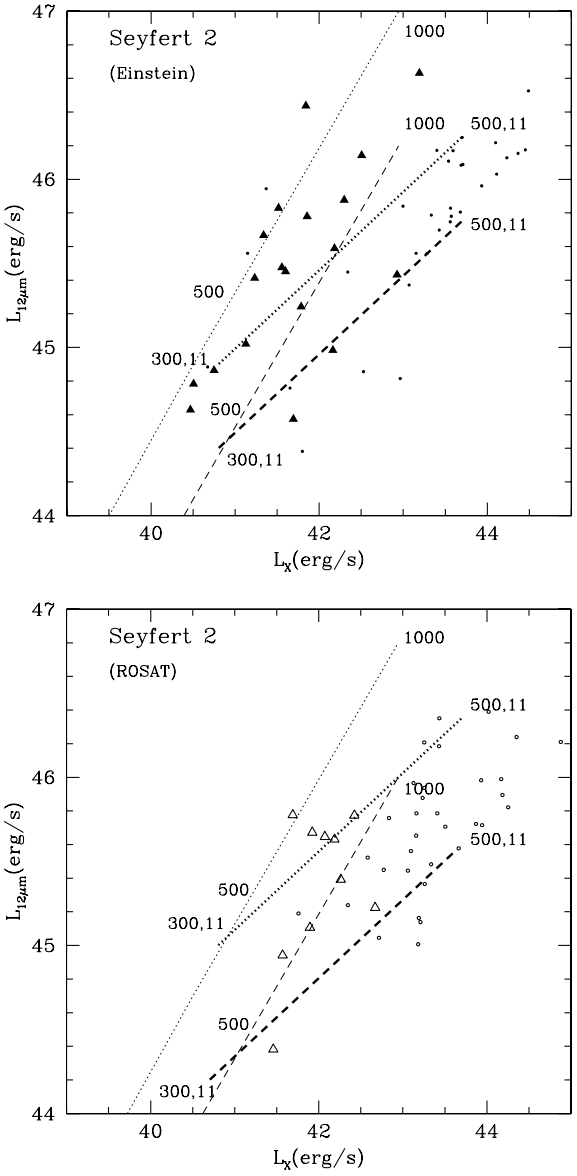

Figure 8. $L_{12\,\mu m}$ versus L_X for Sy2 galaxies (larger symbols). The top panel refers to the *Einstein* sample, while the bottom panel to *ROSAT* sample. The curves are labelled by V_s and log F_h values for RD models and by V_s for SD models. The line types are given in Tables 3 and 4 (last column). The notation for the data is as follows: filled triangles (top panel) represent the *Einstein* sample and open triangles (bottom panel) the *ROSAT* sample; in both panels, tiny symbols correspond to Sy1 data.

lower limit, in order to find out the whole range of d/g values for both Sy1s and Sy2s.

The theoretical results are represented by lines, labelled by the input parameters V_s for SD models (thin lines), and the pair (V_s, log F_h) in the case of RD models (thick lines). Short dashed lines refer to dust emission in the IR, while long dashed lines refer to IR bremsstrahlung.

Fitting of the observed correlation with our models is not so simple. First, recall that models correspond to single clouds (see Section 3.2). Thus, the comparison between the theoretical and observational data can only give a rough indication of the physical conditions of the gas and of the velocity field of the clouds emitting soft X-rays. Secondly, as already commented above (Section 3.1), in order to derive the luminosities, the fluxes calculated by the models must be multiplied by a factor (η) that represents the fraction of the observed luminosity coming from a specific type of cloud, characterized by V_s, n_0 and F_h. If the infrared emission is due to dust, this factor must also account for the differences of the dust-to-gas ratio assumed in the calculations and the real value for each galactic nucleus. A higher d/g value leads to an enhancement of the L_{IR} emission. Thus, we expect that the η factor is not constant but may have different values for different galaxies. It could be empirically obtained by fitting the observed emission-line and continuum spectra with a multi-cloud model, as already presented for Circinus and NGC 5252 (Contini et al. 1998a,b).

Table 3. The logarithm of the η factors using the *Einstein* data.

Type	Model	X-ray[a]	IR (br)	IR (dust)	r (pc)	d/g (10^{-14})	Line type
Sy1	RD	43.8	44.2	–	747	–	thick long-dashed
Sy1	SD	42.6	–	46.0	187.6	251	thin short-dashed
Sy1	RD	44.1	–	45.2	1055	1.26	thick short-dashed
Sy2	SD	40.1	–	44.5	10.5	2512	thin short-dashed
Sy2	SD	40.1	–	45.3	10.5	1.58(4)	thin dotted
Sy2	RD	43.3	–	44.8	420	3.16	thick short-dashed
Sy2	RD	43.3	–	45.3	420	10.0	thick dotted

[a]*Einstein* data.

Table 4. The logarithm of the η factors using the *ROSAT* data.

Type	Model	X-ray[a]	IR (br)	IR (dust)	r (pc)	d/g (10^{-14})	Line type
Sy1	RD	44.1	44.1	–	1055	–	thick long-dashed
Sy1	SD	42.5	–	46.2	167.2	501	thin short-dashed
Sy1	RD	43.9	–	44.9	838	1	thick short-dashed
Sy2	SD	40.1	–	44.3	10.5	1585	thin short-dashed
Sy2	SD	40.1	–	45.1	10.5	1.0(4)	thin dotted
Sy2	RD	43.2	–	44.6	374	2.5	thick short-dashed
Sy2	RD	43.3	–	45.4	420	12.6	thick dotted

[1]*ROSAT* data.

Since our goal is to analyse the $L_{12\,\mu m}$–L_X correlation, we try to obtain a rough picture of the physical processes in the active nuclei with a minimum number of input parameters. First, we constrain the models by considering the main trends shown by the data, because these trends define which type of models must be adopted (RD, SD, IR from dust or IR from bremsstrahlung). Then, we shift the model results in order to cover the largest number of data by changing the η factor.

Recall that, in the SED presented in Fig. 1, the high-frequency domain corresponds to the hot gas emission, i.e. even in radiation-dominated models it depends on the shock velocity. So, the soft X-ray emission is due to bremsstrahlung in the shocked zone of high-velocity clouds while its infrared counterpart can contribute to the mid- or near-IR emission. In this case, since both continua come from the same cloud, the corresponding η should be the same.

The logarithm of η for the bremsstrahlung and for dust emission, adopted for modelling the correlations presented in Figs 7 and 8, are given in Tables 3 and 4 for *Einstein* and *ROSAT* data, respectively. In the first column of Tables 3 and 4, the type of the galaxy is given. In the *ROSAT* sample, Sy1 includes the Sy1.5 data. The model type (SD or RD) is indicated in the second column. The logarithm of the η value that provides the best fit of the data by the corresponding model (see line type in column 8) are given in columns 3, 4 and 5 for L_X, $L_{12\,\mu m}$ generated by bremsstrahlung, and $L_{12\,\mu m}$ by dust, respectively. In columns 6 and 7 the calculated distance of the emitting clouds from the AC (assuming a covering factor equal to unity) and the d/g ratio by number are given, respectively. The values of d/g by number that better fit the data are calculated from the difference between η corresponding to IR (dust) and η corresponding to X-rays for each type of galaxy in Tables 3 and 4. The line type used to draw the curves corresponding to the models (Figs 7 and 8) are listed in the last column.

4.2 Type 1 Seyfert galaxies

Two clear trends are present in Fig. 7 (top panel) corresponding to the Sy1 *Einstein* sample: (a) Sy1s with $L_X \leqslant 3 \times 10^{43}$ show a larger scatter of the $L_{12\,\mu m}$ values; and (b) the objects with higher L_X values are mainly located between RD (thick short-dashed line) and SD (thin short-dashed line) models both with IR due to dust emission. The results corresponding to $L_{12\,\mu m}$ due to bremsstrahlung (thick long-dashed line) could eventually explain some Sy1 and Sy2 data.

Regarding the *ROSAT* data (Fig. 7, bottom panel), most of the data are also inside a sector defined by RD models (lower edge) and SD models (upper edge), as found for the *Einstein* sample. High $L_{12\,\mu m}$ Sy1 galaxies are better fitted by dust emission from SD models with $300 < V_s \leqslant 1000$ km s^{-1} (thin line), whereas those with low $L_{12\,\mu m}$ would be dominated by dusty RD clouds with $F_h = 10^{11-12}$ (cm^{-2} s^{-1} eV^{-1}) and V_s in the range 300–500 km s^{-1}. Also for the *ROSAT* data, the line corresponding to the IR bremsstrahlung emission fits some Sy1 and Sy2 data, but not the trend of the Sy1 complex.

4.3 Type 2 Seyfert galaxies

The sample of Sy2s is shown in Fig. 8 for both *Einstein* (top panel) and *ROSAT* data (bottom panel). In both samples, the data are better explained by RD or SD models with $L_{12\,\mu m}$ produced by dust thermal emission. The notation is the same as in Fig. 7. Notice that thin short-dashed lines refer to SD models and thick short-dashed to RD models with IR from dust, while dotted lines correspond to the same models shifted in the diagrams towards higher L_{IR}, in order to explain the high IR luminosity of objects that are rich in dust.

Except for four objects in the top panel and three in the bottom panel, most of the data points are located between two SD curves, characterized by log $\eta = 40.1$ and 43.3. On the other hand, the objects on the right of the SD curves are close to the RD results (thick short-dashed line) with log $F_h = 11$, V_s between 300 and 500, and a relatively low d/g (see Tables 3 and 4).

4.4 Discussion

The first results of our investigation show that the X-ray and near-IR correlation for Sy1s can be explained by the composite models of clouds producing both bremsstrahlung and dust emission. In the

diagrams these models cover most of the area where the AGN data points are distributed.

In a photoionized zone, the dust cannot reach a temperature high enough to contribute to the 12 μm emission, whereas a shocked zone may heat the dust to higher temperatures, as shown in Table 1. Therefore, models accounting for the shock are important. Considering the whole sample for a given class (Sy1 or Sy2), the contribution of RD and SD clouds to the IR emission coming from thermal emission by dust provides the best fit to the correlation for both *Einstein* and *ROSAT* data.

The values of the factor η adopted for the models and presented in Tables 3 and 4 give a rough estimation of the distance of the emitting nebula from the AC. Notice, however, that the observed L_X may include a contribution from the central source, while $L_{12\,\mu m}$ depends on d/g. So, the η value corresponding to $L_{12\,\mu m}$ due to bremsstrahlung, which is related to the distance of the cloud to the AC, can be lower than that corresponding to L_X.

The ratio of η for L_X and $L_{12\,\mu m}$ will provide an estimate of the L_X emitted from the AC relative to L_X emitted by bremsstrahlung. For example, the observational data (*Einstein* sample) for the Sy1 galaxy Mrk 335 could be reproduced by IR from dust with a high d/g. However, it could also be reproduced by IR produced by bremsstrahlung, with $\log(\eta)_{\rm soft\,X} = 43.7$ and $\log(\eta)_{\rm IR} = 43.6$. A difference in the η values showing $\log(\eta)_{\rm soft\,X}$ higher than $\log(\eta)_{\rm IR}$ indicates a contribution from the AC to L_X. In this case, this galaxy could show soft X-ray short-term variability.

The theoretical results shown in Figs 7 and 8 correspond to models with $d/g = 10^{-15}$. With a lower d/g, $L_{12\,\mu m}$ dust will hardly prevail over $L_{12\,\mu m}$ bremsstrahlung; therefore, also in the case of emission by dust, we assume as indicative of the nebula radius the lowest value of η. The Sy2 galaxies included between the thin short-dashed and dotted curves of Fig. 8 have a d/g between 2.5×10^{-12} and 1.6×10^{-11} (*Einstein*) and between 1.6×10^{-12} and 10^{-11} (*ROSAT*). The results for the Sy1 galaxies indicate $d/g = 2.5 \times 10^{-13}$–$1.3 \times 10^{-14}$ (*Einstein*) and 5×10^{-13}–10^{-14} (*ROSAT*).

Regarding the objects with IR coming from dust reradiation, results obtained for the galaxies of both *Einstein* and *ROSAT* samples, we obtain from the values of η listed in Tables 3 and 4 a characteristic distance of a few hundred parsecs to a few kiloparsecs for the Sy1s. The distances for Sy2 galaxies are smaller, going from a few to about 500 pc.

In brief, the results obtained by the modelling the L_X–$L_{12\,\mu m}$ correlation suggest that both SD and RD clouds are present in Sy1s and Sy2s. Notice, however, that for Sy2 galaxies, V_s is about 300 km s^{-1} and log F_h is of the order of 11, while Sy1s have higher V_s (up to 600 km s^{-1}) and higher F_h (log F_h up to 12).

Clouds closer to the nuclear region are shock-dominated because a large amount of dust can prevent the ionizing radiation from the AC. High-velocity ($V_s = 1000$ km s^{-1}) and dust-rich SD clouds are more likely to be present in Sy2s than in Sy1s, and are closer to the centre. This indicates that the emitting region in Sy2s is more compact than in Sy1s. However, the maximum distance of a few kiloparsecs obtained for Sy1s from the fit of the *ROSAT* sample could represent an upper limit if the emitting gas has both a high d/g and a strong contribution to the X-ray coming from the active nucleus. Schmitt et al. (2003) found that both Seyfert types have similar distributions of the NLR sizes, although it is expected that Sy1s have on average smaller NLR sizes than Sy2s (Mulchaey, Wison & Tsvetanov 1996). Notice that Schmitt et al. claim that there are 'effects which could alter both the measurements and models'.

Finally, the results obtained from the ensemble of Seyfert galaxies reveal that the X-ray–near-IR emitting regions of Sy1s and Sy2s have indeed different characteristics, which are hardly noticeable when modelling single objects.

5 CONCLUDING REMARKS

In this paper we looked for new evidence for differences in parameter ranges characterizing the NLR of Sy1s, Sy2s and LINERs (and LLAGNs) by modelling of the L_X–$L_{12\,\mu m}$ correlation by composite models accounting for dust emission.

Soft X-rays are considered because they show less dramatic variability. In our models, soft X-rays are emitted in the post-shock region of clouds with relatively high shock velocities. Dust and gas are coupled crossing the shock front, and therefore dust emission from the cloud region that emits the soft X-rays peaks in the mid-IR. Shocks are relatively important in modelling the LLAGN spectra, so we started our investigation with the L_{IR}–L_X correlation for LLAGNs. The results are sensitive enough to apply the same modelling method to Seyfert galaxies.

We found that shock velocities are between 300 and 1000 km s^{-1} for all the objects, lower in LLAGNs and Sy2s, higher in the NLR of Sy1 galaxies. The intensity of the flux from the AC is low for LINERs and LLAGNs (log $F_h = 9$–10) and increases towards Sy2s (log $F_h \simeq 11$), being higher for Sy1s (log $F_h \leqslant 12$). Results obtained by modelling the *Einstein* sample and the *ROSAT* sample are in full agreement. Dust-to-gas ratios by number are larger than 10^{-14} (4×10^{-4} by mass) for LINERs and LLAGNs, between 10^{-14} and 3×10^{-13} (4×10^{-4} and 0.012 by mass) for Sy1s, and reach 2×10^{-11} (0.8 by mass) for Sy2s.

The soft X-ray variability of Seyfert galaxies can be inferred from the η values deduced from the models. If $(\eta)_{\rm IR} < (\eta)_{\rm soft\,X}$ there is a strong contribution of soft X-rays from the AC to the observed value. Therefore, objects of the sample used in this paper which could present strong variability can be identified.

ACKNOWLEDGMENTS

We are very grateful to an unknown referee for valuable comments. This paper is partially supported by FAPESP (00/06695-0), CNPq (304077/77-1).

REFERENCES

Allen C. W., 1973, Astrophysical Quantities. Athlone Press, University of London
Antonucci R. R. J., Miller J. S., 1985, ApJ, 297, 621
Barvainis R., 1990, ApJ, 297, 621
Becker R. H., White R. L., Edwards A. L., 1991, ApJS, 75, 1
Becker R. H., White R. L., Helfand D. J., 1995, ApJ, 450, 559
Carleton N. P., Elvis M., Fabbiano G., Willner S. P., Lawrence A., Ward M., 1987, ApJ, 318, 595
Condon J. J., Condon M. A., Broderick J. J., Davis M. M., 1983, AJ, 88, 20
Contini M., 1997, A&A, 323, 71
Contini M., Viegas S. M., 1999, ApJ, 523, 114
Contini M., Viegas S. M., 2000, ApJ, 535, 721
Contini M., Viegas S. M., 2001, ApJS, 132, 211
Contini M., Prieto A. M., Viegas S. M., 1998a, ApJ, 492, 511
Contini M., Prieto A. M., Viegas S. M., 1998b, ApJ, 505, 621
Contini M., Viegas S. M., Prieto M. A., 2002, A&A, 386, 399
Douglas J. N., Bash F. N., Bozyan F. A., Torrence G. W., Wolfe C., 1996, AJ, 111, 1945
Dressel L. L., Condon J. J., 1978, ApJS, 36, 53
Ekers J. A., 1969, Aust. J. Phys. Suppl. 7, 1

Ficarra A., Grueff G., Tomasetti G., 1985, A&AS, 59, 255
Giuricin G., Tamburini L., Mardirossian F., Mezzetti M., Monaco P., 1994, ApJ, 427, 202
Giuricin G., Mardirossian F., Mezzetti M., 1995, ApJ, 446, 550
Gower J. F. R., Scott P. F., Wills D., 1967, Mem. R. Astron. Soc., 71, 49
Green P. J., Anderson S. F., Ward M. J., 1992, MNRAS, 254, 30
Gregory P. C., Condon J. J., 1991, ApJS, 75, 1011
Halderson E. L., Moran E. C., Filippenko A. V., Ho L. C., 2001, ApJ, 122, 637
Heeschen D. S., Wade C. M., 1964, AJ, 69, 277
Ho L. C., Filippenko A. V., Sargent W. L. W., 1997, ApJ, 487, 568
Israel F. P., Mahoney M. J., 1990, ApJ, 352, 30
Iwasawa K., Wilson A. S., Fabian A. C., Young A. J., 2003, astro-ph/0306139
Kellermann K., Pauliny-Toth I., Williams P., 1969, ApJ, 157, 1
Kuhr H., Witzel A., Pauliny-Toth I. I. K., Nauber U., 1981, A&AS, 45, 367
Laing R. A., Peacock J. A., 1980, MNRAS, 190, 903P
Large M. I., Mills B. Y., Little A. G., Crawford D. F., Sutton J. M., 1981, MNRAS, 194, 693P
Moran E. C., Halpern J. P., Helfand D. J., 1996, ApJSS, 106, 341
Mulchaey J. S., Wison A. S., Tsvetanov Z. I., 1996, ApJ, 467, 197
Pounds K. A., Warwick R. S., Culhane J. L., de Korte P. A. J., 1986, MNRAS, 218, 685
Rodriguez-Ardila A., Viegas S. M., Pastoriza M. G., Prato L., 2002, ApJ, 579, 214
Schmitt H. R., Donley J. L., Antonucci J. B., Hutchings A. L., Kinney A. L., Pringle J. E., 2003, astro-ph/0307255
Spoon H. W. W., Keane J. V., Tielens A. G. G. M., Lutz D., Moorwood A. F. M., Laurent O., 2002, A&A, 385, 1022
Terashima Y., Ho L. C., Ptak A. F., 2000, ApJ, 533, 729
Terashima Y., Iyomoto N., Ho L. C., Ptak A. F., 2002, ApJS, 139, 1
Viegas S. M., Contini M., 1994, ApJ, 428, 113
Viegas S. M., de Gouveia dal Pino E. M., 1992, ApJ, 384, 467
Viegas-Aldrovandi S. M., Contini M., 1989, ApJ, 339, 689
Waldram E. M., Yates J. A., Riley J. M., Warmer P. J., 1996, MNRAS, 282, 779
White R. L., Becker R. H., 1992, ApJS, 79, 331
Wright A., Otrupcek R., 1990, Parkes Catalog, Aust. Tel. National Facility

This paper has been typeset from a TEX/LATEX file prepared by the author.